Investigation of the molecular structure of 4-(3-methyl-3-phenylcyclobutyl)-2-[2-(3-methylbenzylidene)hydrazinyl]thiazole in the gas and solid phases

Article *in* Acta crystallographica. Section C · November 2018

DOI: 10.1107/S2053229618013475

CITATIONS
5

READS
127

1 author:

Tuncay Karakurt
Ahi Evran Üniversitesi
44 PUBLICATIONS **241** CITATIONS

SEE PROFILE

STRUCTURAL CHEMISTRY

ISSN 2053-2296

Investigation of the molecular structure of 4-(3-methyl-3-phenylcyclobutyl)-2-[2-(3-methylbenzylidene)hydrazinyl]thiazole in the gas and solid phases

Tuncay Karakurt*

Department of Chemical and Process Engineering, Faculty of Engineering–Architecture, Ahi Evran University, Kirsehir 40100, Turkey. *Correspondence e-mail: tuncaykarakurt@gmail.com

Received 28 August 2018
Accepted 20 September 2018

Edited by P. Fanwick, Purdue University, USA

Keywords: Schiff base; DFT; tautomer; PBC; quantum ESPRESSO; crystal structure.

CCDC reference: 1830817

Supporting information: this article has supporting information at journals.iucr.org/c

In this study, the title Shiff base, $C_{22}H_{23}N_3S$, was synthesized and examined by ^1H and ^{13}C NMR spectroscopy and X-ray analysis techniques. The crystal structure is stabilized by classical intermolecular N—H···N hydrogen bonding. The crystal packing is additionally stabilized by C—H···π interactions. It has been observed that the compound can exist in two different tautomeric forms, and experimental and theoretical studies were carried out on these tautomeric structures. For this purpose, the gas phase of the compound was optimized by density functional theory (DFT) using the B3LYP/6-311G(d) method, which allowed for the structural parameters (bond angles, bond lengths and dihedral angles), as well as the frontier molecular orbitals (FMO), to be examined. In addition, stable structures of the two tautomers in the solid phase were obtained using *Quantum ESPRESSO* under periodic boundary conditions (PBC).

1. Introduction

Schiff base containing compounds with a double bond (N═C) are used as starting materials in the synthesis of important drugs, especially antibiotics, antiallergics, antiphlogistics, and anticancer, antioxidant and antitumour drugs (O'Neil *et al.*, 2001; Ayhan-Kılcıgil *et al.*, 2007; Kus *et al.*, 2004). These compounds have exhibited photochromism and thermochromism, and the photochromism properties have been used to measure and control radiation intensity, image systems and optical computers (Karakurt *et al.*, 2016). The azomethine and imine derivatives of Schiff bases are organic intermediates commonly used in the production of pharmaceutical or rubber additives (Macho *et al.*, 2004). Schiff bases are also used in the paint industry because they are transparent, solid and coloured. In analytical chemistry, they have been used as spectrophotometric reagents due to their selective and specific reactions with certain metal ions (Issaadi *et al.*, 2011). Copper(II) complexes formed from Schiff base ligands have been important model compounds in studying the chemical and physical behaviour of biological copper systems (Reddy *et al.*, 2000). Thiazole and its derivatives are important in biological systems such as anti-inflammatory and analgesic (pain killer) agents for lipoxygenase enzyme activities and inhibitors (Hadjipavlou-Litina & Geronikaki, 1996; Holla *et al.*, 2003). This compound can also be found in the composition of fungicides and insecticides. Schiff bases have been used as substrates in the preparation of the majority of industrial and biologically active compounds *via* regeneration and ring-addition reactions (Jarahpour *et al.*, 2004).

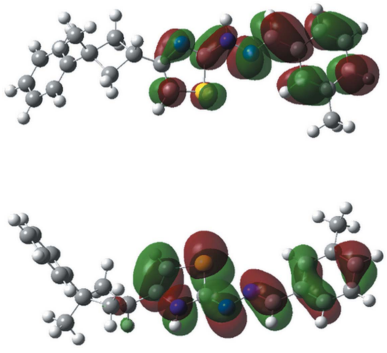

In thiazole and its derivatives, depending on whether the N atom is cationic, the benzothiazolium group is used as an electron donor or electron acceptor in the paint industry, and it is also used for agricultural purposes due to its fungicidal properties (Zollinger, 2003; Shyam & Tiwari, 1975). Aminothiazoles are used as starting materials in the synthesis of many analgesics and antipyretics in pharmacy, and their antiviral, antimicrobial and antibacterial properties have been proven by many studies (Nagatomi & Ando, 1984; Kutter *et al.*, 1972).

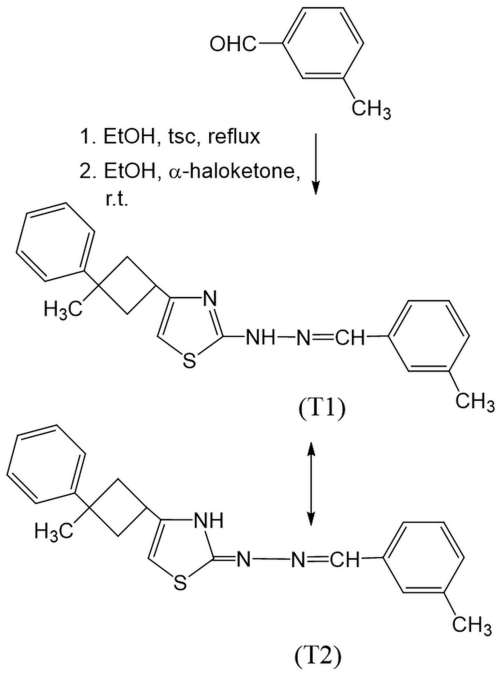

Scheme 1

A cyclobutane substituent enables the molecule to adopt a more stable conformation by puckering. Although puckering causes the tension to increase by reducing the C—C—C angles, it reduces the total tension by decreasing the adjacent hydrogen overlap (Hart, 1995).

In the light of the biological effects mentioned above, the structure of the new Schiff base 4-(3-methyl-3-phenylcyclobutyl)-2-[2-(3-methylbenzylidene)hydrazinyl]thiazole was confirmed by IR, ^{1}H NMR, ^{13}C NMR and X-ray diffraction techniques. The single crystal, which may be in two tautomeric structures, has been studied both experimentally and theoretically. The minimum-energy values of the two tautomeric structures in the gas phase were calculated using the *GAUSSIAN09* program (Frisch *et al.*, 2009) and the lattice energies in the solid phase of the two tautomeric structures. This was carried out under periodic boundary conditions (PBC), which were calculated using the *Quantum ESPRESSO 6.2.1* package (https://www.quantum-espresso.org/).

2. Experimental

2.1. Synthesis and crystallization

The starting materials 3-methylbenzaldehyde and thiosemicarbazide were purchased from Merck and used as received. The α-haloketone 3-(2-chloro-1-oxoethyl)-1-methyl-1-phenylcyclobutane was synthesized according to a literature procedure (Akhmedov *et al.*, 1991). A mixture of 3-methylbenzaldehyde (1.2015 g, 10 mmol) and thiosemicarbazide (0.9114 g, 10 mmol) in ethanol (10 ml) was refluxed for 2 h. Subsequently, a solution of α-haloketone (2.2271 g, 10 mmol) in ethanol (20 ml) was added dropwise at room temperature and the mixture was stirred for 3 h (thin-layer chromatography). A dark-yellow precipitate was obtained, filtered off, washed with copious amounts of water several times, dried in air and crystallized from EtOH (Scheme 1) (yield: 73%; m.p. 427 K). Characteristic IR bands (cm^{-1}): 3148 ν(–NH–), 3120 ν(N—H), 1567 ν(C═N thiazole), 1536 ν(C═N azomethine), 705 ν(C—S—C thiazole). Characteristic ^{1}H NMR shifts ($CDCl_3$, δ, ppm): 1.56 (*s*, 3H, –CH_3), 2.42 (*s*, 3H, –CH_3), 2.54 (*s*, 2H, –CH_2–, cyclobutane), 2.56 (*m*, 2H, –CH_2–, cyclobutane), 3.67–3.71 (quint, J = 7.2 Hz, 1H, >CH–, cyclobutane), 6.27 (*d*, J = 0.8 Hz, 1H, aromatic), 7.19–7.21 (*m*, 4H, aromatics), 7.31–7.36 (*m*, 3H, aromatics), 7.51 (*m*, 2H, aromatics), 7.79 (*s*, 1H, azomethine), 9.62 (*s*, 1H, –NH–). Characteristic ^{13}C NMR shifts ($CDCl_3$, δ, ppm): 168.66, 156.11, 152.28, 141.67, 138.41, 134.06, 130.39, 128.62, 128.24, 127.16, 125.34, 124.76, 124.09, 102.07, 40.23, 38.88, 30.84, 30.17, 21.41.

Table 1
Experimental details.

Crystal data	
Chemical formula	$C_{22}H_{23}N_3S$
M_r	361.49
Crystal system, space group	Monoclinic, *C*2/*c*
Temperature (K)	296
a, *b*, *c* (Å)	20.135 (6), 6.826 (2), 29.027 (9)
β (°)	100.759 (14)
V (Å^3)	3920 (2)
Z	8
Radiation type	Mo $K\alpha$
μ (mm^{-1})	0.18
Crystal size (mm)	0.30 × 0.25 × 0.20
Data collection	
Diffractometer	Bruker APEXII CCD area-detector
No. of measured, independent and observed [$I > 2\sigma(I)$] reflections	37086, 4808, 3768
R_{int}	0.030
(sin $\theta/\lambda)_{max}$ (Å^{-1})	0.671
Refinement	
$R[F^2 > 2\sigma(F^2)]$, $wR(F^2)$, S	0.053, 0.139, 1.07
No. of reflections	4808
No. of parameters	241
H-atom treatment	H atoms treated by a mixture of independent and constrained refinement
$\Delta\rho_{max}$, $\Delta\rho_{min}$ (e Å^{-3})	0.26, −0.22

Computer programs: *APEX2* (Bruker, 2008), *SAINT* (Bruker, 2008), *SHELXT2014* (Sheldrick, 2015*a*), *SHELXL2016* (Sheldrick, 2015*b*), *Mercury* (Macrae *et al.*, 2008) and *OLEX2* (Dolomanov *et al.*, 2009).

2.2. Computational details

The optimization of the title molecule in the gas phase and calculation of its geometrical parameters were carried out using *GAUSSIAN09* (Frisch *et al.*, 2009) software employing

the B3LYP (Becke, 1993, Lee *et al.*, 1988) method and the 6-311g(d) (Foresman & Frisch, 1996) basic set. The results were visualized using the *Gausview 5* (Dennington *et al.*, 2009) program. Calculations in the crystal phase were performed with the *Quantum ESPRESSO* program, which uses periodic boundary conditions. In this calculation, the following were used: density functional theory (DFT) (Hohenberg & Kohn, 1964, Kohn, 1965), which is based on plane waves, local density approximation (LDA) under Perdew–Zung's (PZ) pseudo-potential (Perdew, 1981), and one of *Quantum ESPRESSO* basic components of the *PWscf* (plane waves self-consistent field) (Giannozzi *et al.*, 2009) program set.

2.3. Refinement

Crystal data, data collection and structure refinement details are summarized in Table 1. The positions of H atoms connected to C atoms were determined geometrically. The bond lengths of the aromatic, methylene and methyl C—H groups were fixed at 0.93, 0.97 and 0.96 Å, respectively. The H atoms were refined with common isotropic displacement parameters, with U_{iso}(H) = 1.2U_{eq}(C) for the aromatic and methylene protons, and 1.5U_{eq}(C) for the methyl protons. The H atom on the thiazole N atom was located in a difference Fourier map and refined isotropically. The N2—H2 distance was restrained to 0.95 (2) Å.

3. Results and discussion

3.1. Geometrical structure of title compound

Fig. 1(*a*) displays the H-atom electron-density difference of the crystal structure of **T2** in the asymmetric unit. The red colour indicates areas where the electron density is too high, while the green networks display holes. In this case, the H atom in the **T2** structure can be said to be in the wrong

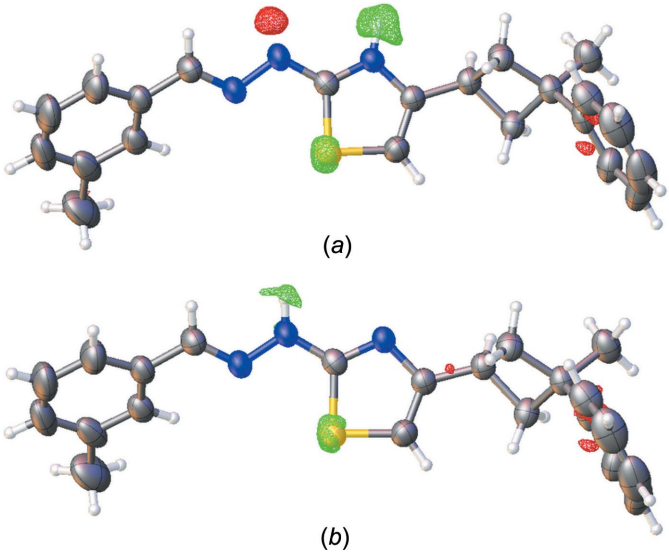

Figure 1
An early refinement state of the title compound showing the difference electron density. Missing (green) and erroneously placed (red) H atoms are clearly visible.

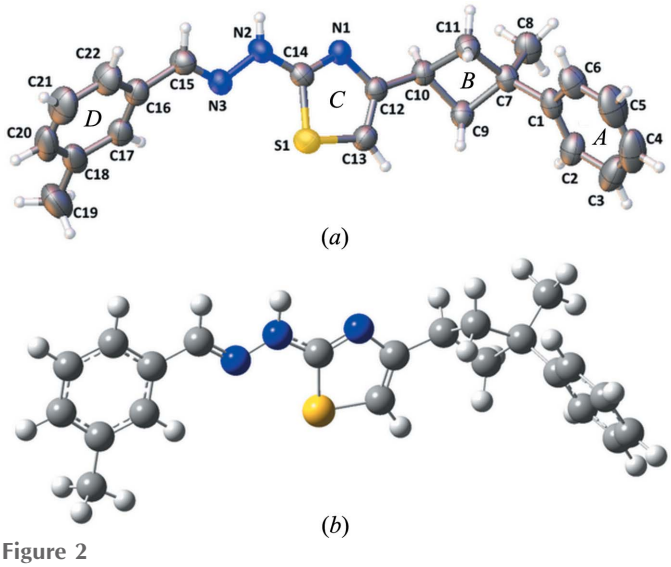

Figure 2
(*a*) Experimental (20% probability displacement ellipsoids) and (*b*) calculated figures of the title crystal in the **T1** form.

position. In Fig. 1(*b*), it can be seen that the H atom in the **T1** structure is positioned correctly. The **T1** form can be seen to be the more stable. A displacement ellipsoid plot of the title molecule is shown in Fig. 2(*a*) and the optimized molecule obtained by *GAUSSIAN09* (Frisch *et al.*, 2009) is shown in Fig. 2(*b*).

As can be seen from Fig. 2(*a*), the **T1** form consists of a benzene ring (*A*, atoms C1–C6), a cyclobutane ring (*B*, C7–C11), a thiazole ring (*C*, C12/C13/S1/C14/N1) and a toluene ring (*D*, C16–C22). Each of these rings is approximately planar and the largest deviations from planarity were 0.011, 0.119, 0.004 and 0.014 Å, respectively. In addition, the dihedral angles between these four rings were *A*/*B* = 40.44 (2), *B*/*C* = 51.52 (2) and *C*/*D* = 49.16 (2)°. Due to steric interactions between the side groups, the cyclobutane ring is puckered and deviates from planarity [puckering angle = 24.7 (2)°, shown in Fig. 3 for the planes C11/C7/C9 and C9–C11].

This bending angle is reported in the literature as 23.05 (4)° (Swenson *et al.*, 1997). The X-ray diffraction analysis of the **T1** form and some geometric parameters (bond lengths, bond angles and torsion angles), which have been calculated in the gas and solid phases, are given in Table 2.

When the X-ray diffraction results of the stable **T1** form of the crystal were analysed, it was seen that, as expected, the N1═C14 double bond in the thiazole ring is shorter than the N1—C12 single-bond length. These bond lengths were found to be 1.302 (2) and 1.399 (2) Å, respectively. The C12═C13 bond length, which displays double-bond character, is 1.341 (3) Å, and the S1—C13 and S1—C14 bond lengths are 1.728 (2) and 1.732 (2) Å, respectively. These bond lengths are shorter than the value of 1.76 Å (Allen, 1984) which is accepted in the literature for a S—Csp^2 bond, but is in accordance with the values given in the literature for the thiazole ring (Özdemir, 2013) due to delocalization of two lone pairs of electrons on the S1 atom between the C13 and C14 atoms. The title crystal displays no intramolecular

Table 2
Calculated and experimental (exptl) geometric parameters (Å, °) of the crystal in the **T1** form.

	Exptl (**T1** form)	Exptl (**T2** form)	Gaussian-DFT [B3LYP/6-311G(d)] (**T1** form)	*Quantum ESPRESSO* (**T1** form)
Bond lengths				
C1—C2	1.381 (3)	1.383 (4)	1.399	1.391
C1—C6	1.385 (3)	1.384 (4)	1.399	1.388
C6—C5	1.378 (4)	1.384 (4)	1.393	1.386
C12—C13	1.341 (3)	1.339 (3)	1.360	1.361
S1—C14	1.732 (2)	1.734 (2)	1.756	1.730
S1—C13	1.728 (2)	1.728 (2)	1.752	1.717
N1—C12	1.399 (2)	1.395 (2)	1.386	1.379
N1—C14	1.302 (2)	1.298 (3)	1.298	1.312
N2—C14	1.360 (2)	1.362 (3)	1.372	1.345
C10—C9	1.538 (3)	1.537 (3)	1.549	1.527
C10—C11	1.557 (3)	1.558 (3)	1.558	1.546
C12—C10	1.482 (3)	1.483 (3)	1.495	1.472
C7—C9	1.554 (3)	1.555 (3)	1.565	1.543
C7—C11	1.544 (3)	1.542 (3)	1.564	1.538
N2—N3	1.379 (2)	1.387 (3)	1.344	1.335
N3—C15	1.266 (3)	1.266 (3)	1.284	1.285
Bond angles				
C15—N3—N2	117.1 (2)	116.6 (2)	118.4	118.11
C14—N2—N3	114.8 (1)	114.1 (2)	121.4	115.90
N1—C14—N2	125.1 (2)	125.1 (2)	122.3	125.85
N1—C14—S1	116.0 (1)	115.5 (1)	116.0	115.33
C13—S1—C14	88.14 (9)	88.2 (1)	87.3	88.35
C2—C1—C6	118.0 (2)	118.2 (2)	118.1	118.82
C11—C7—C9	88.0 (1)	88.0 (2)	87.8	88.33
C10—C9—C7	89.4 (1)	89.4 (2)	89.2	89.0
Torsion angles				
N1—C12—C10—C9	−178.8 (2)	−178.8 (2)	174.2	179.83
N1—C12—C13—S1	−0.4 (2)	−0.4 (2)	−0.1	0.79
N3—C15—C16—C17	−27.8 (3)	−27.9 (3)	0.1	27.17
C12—N1—C14—S1	0.5 (2)	0.4 (2)	−0.2	−1.59
C14—S1—C13—C12	0.6 (1)	0.5 (2)	−0.1	−1.35

hydrogen bonds. An intermolecular N2—H2···N1^{i} hydrogen bond (Table 3) generates an $R_2^2(8)$ dimer motif (Fig. 4).

In addition, there are three weak C—H···*Cg* (π-ring) interactions in the molecular arrangement within the crystal. These interactions were comprised of C4 and C13 atoms at (x, y, z) with the centre of mass of the toluene ring (centre of mass fractional coordinates: 0.6639, 0.2840, 0.6918 for the C4 atom and −0.6639, 0.2840, −0.6918 for C13 atothe m) and of the C10 atom with the centre of mass of the thiazole ring (centre of mass fractional coordinates: −0.2626, −0.4233, −0.8671). The symmetry information about the hydrogen bonding is given in Table 3. The interactions and packaging are shown in Fig. 5.

Table 3
Hydrogen-bond geometry for the crystal in the **T1** form (Å, °).

*Cg*3 and *Cg*4 are the centroids of the S1/C13/C12/N1/C14 and C16–C22 rings, respectively.

D—H···*A*	*D*—H	H···*A*	*D*···*A*	*D*—H···*A*
N2—H2···N1^{i}	0.95 (2)	2.13 (2)	3.067 (2)	169.6 (18)
C4—H4···*Cg*4^{ii}	0.93	2.99	3.797 (3)	146
C10—H10···*Cg*3^{iii}	0.98	2.82	3.605 (2)	137
C13—H13···*Cg*4^{iv}	0.93	2.91	3.657 (2)	139

Symmetry codes: (i) $-x+\frac{3}{2}, -y+\frac{1}{2}, -z+1$; (ii) $x, -y+1, z-\frac{1}{2}$; (iii) $-x+\frac{3}{2}, -y+\frac{3}{2}, -z+1$; (iv) $-x+1, -y+1, -z+1$.

3.2. Tautomerism

With the theoretical calculations, it was observed that the molecule could be in two tautomer forms, *i.e.* **T1** and **T2** (Scheme 1). The geometrical parameters of these two tautomeric structures and the transition state (TS) of the title molecule were calculated using the DFT/B3LYP/6-311G(d) level of theory. The tautomeric structure energies and the activation energies of the forward–backward reactions are given in Table 4. The imaginary vibration frequency of the transition state of the title molecule was calculated as 1873 cm^{-1}.

The tautomeric forms **T1** and **T2** can be transformed into each other by an intramolecular proton-transfer reaction. Some changes may occur in the structure due to the migration of the H atom from the N atom to the O atom, or from the O atom to the N atom. As shown in Table 4, when the proton was transferred from the **T1** form to the **T2** form, the N2—C14 bond length increased, while the N1—C14 bond length and the N1—C14—N2, N3—N2—C14 and C15—N3—N2 angles decreased. In Fig. 6, where the energy profile of the proton-transfer process is shown, the energy difference between **T1** and **T2** is calculated as being −46.28 kJ mol^{-1} for the gas phase, indicating the greater stability of the **T1** form over the

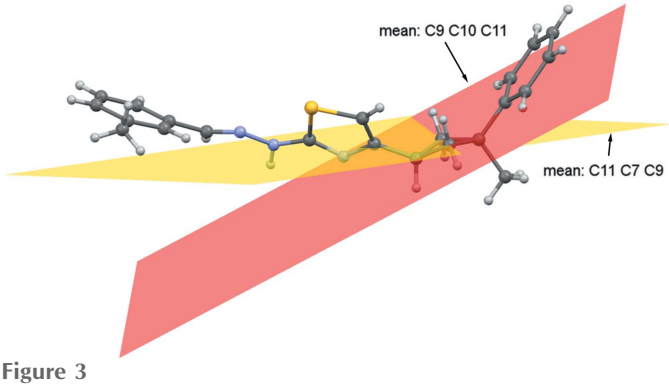

Figure 3
Diagram showing the angle between of the C9–C11 and C11/C7/C9 planes in the cyclobutane rings of the crystal.

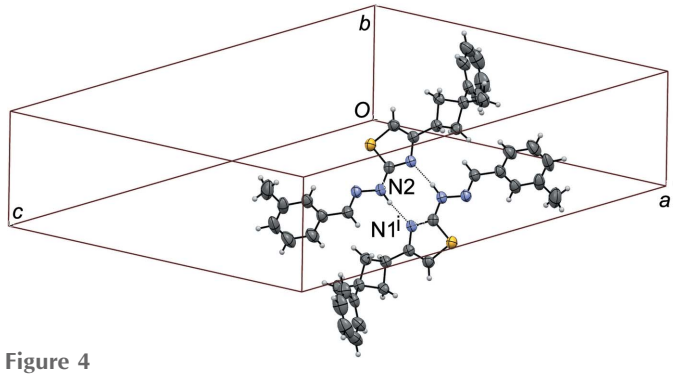

Figure 4
Diagram showing the dimer structure formed by hydrogen bonding. [Symmetry code: (i) $-x+\frac{1}{2}, -y+\frac{1}{2}, -z+1$.]

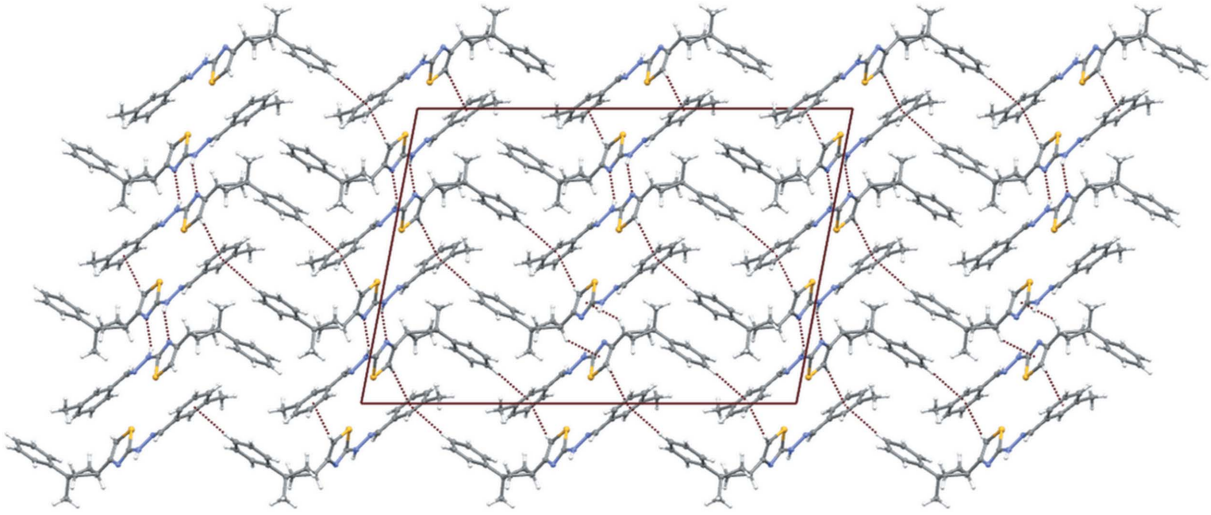

Figure 5
Packing of the crystal in the **T1** form *via* N—H···N and C—H···*Cg* interactions (dashed lines) along the *c* axis.

Table 4
Energies of the **T1** and **T2** forms of the title compound (Hartrees), and energy differences and activation energies.

T1 (a.u.)	**T2** (a.u.)	TS (a.u.)	ΔE (kJ mol^{-1})	$E_a(f)$ (kJ mol^{-1})	$E_a(r)$ (kJ mol^{-1})
−1414.826434	−1414.808633	−1414.747792	−46.28	158.19	204.47

Notes: $\Delta E = E_{keto} - E_{enol}$, $E_a(f)$ = forward activation energy and $E_a(r)$ = reverse activation energy.

Table 5
Comparison of the experimental and optimized unit-cell parameters calculated by the *Quantum ESPRESSO* (QE) VC-Relax method for the **T1** form of the title crystal.

Parameter	Experimental	QE VC-Relax/DFT
Space group	*C*2/*c*	*C*2/*c*
a (Å)	20.135 (6)	19.181
b (Å)	6.826 (2)	6.874
c (Å)	29.027 (9)	28.273
α (°)	90	90
β (°)	100.759 (14)	103.237
γ (°)	90	90
Z	4	4
V (Å^3)	3920 (2)	3629

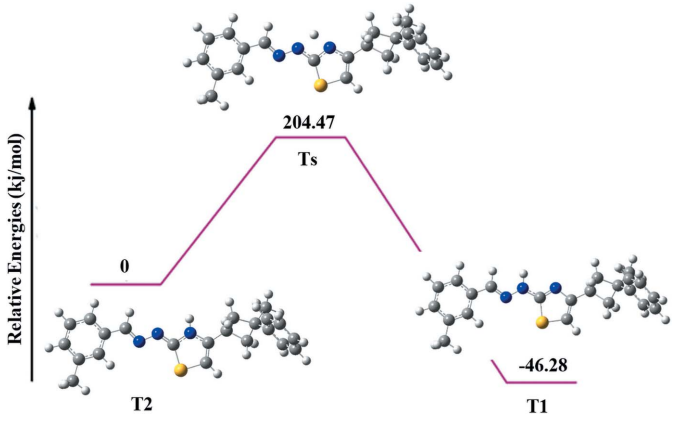

Figure 6
Potential energy diagram for the direct **T1**–**T2** tautomerism of the title compound (asymmetric unit).

T2 form. The relative energy of the transition state, according to the **T1** form, was 158.19 kJ mol^{-1} in the gas phase, while the back-reaction barrier energy was calculated as being 204.47 kJ mol^{-1}. If we look at Table 4, these high barrier energies show that there is unfavourable tautomerism (Atkins, 2006) and a considerably high energy is required for both forward and backward proton transfer. According to these results, it can be said that the **T1** form is more stable than the **T2** form, and is closer to the structure clarified by X-ray diffraction.

3.3. Frontier molecular orbitals

These orbitals describe intramolecular interactions. The energy difference between these two orbitals is a measure of

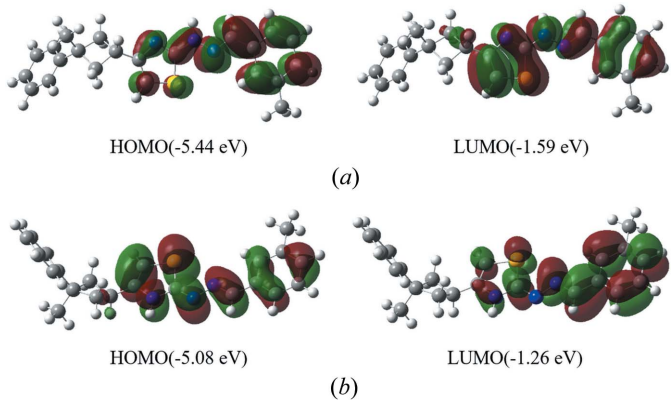

Figure 7
Crystalline gas-phase frontier orbitals and energies for (*a*) **T1** and (*b*) **T2**.

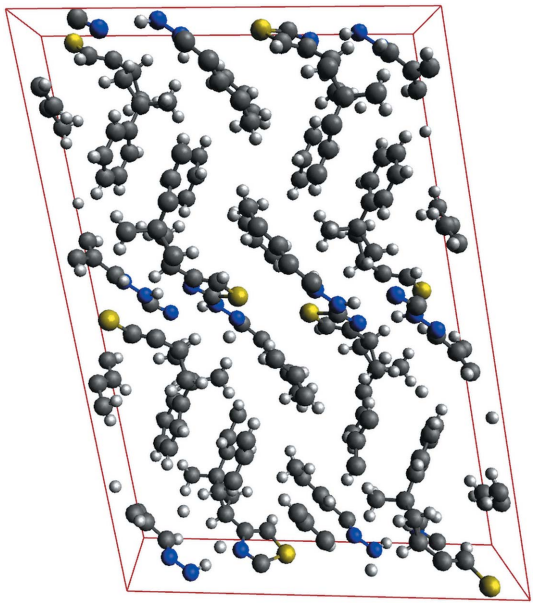

Figure 8
Representation of the atoms in the unit cell of the **T1** form.

the chemical stability of the molecule and this is due to the fact that it is a measure of electron conductivity, which is a critical parameter in determining the properties of molecular electrical transport. This energy difference is largely responsible for the chemical and spectroscopic properties of molecules (Karakurt *et al.*, 2018).

The HOMO (highest occupied molecular orbital) and LUMO (lowest unoccupied molecular orbital) energy values of both tautomeric structures were studied. The HOMO and LUMO energy values of the molecule in the **T1** form are shown in Fig. 7, and the difference between these two orbitals ($\Delta E = E_{\rm LUMO} - E_{\rm HOMO}$) was calculated as 3.85 eV for the **T1** form and 3.82 eV for the **T2** form. The ΔE value calculated for the **T1** form is larger than that of the **T2** form, which indicates that the **T1** form is more stable.

3.4. Periodic boundary calculations (PBC)

The coordinates of the 392 atoms in the unit cell of the crystal in the **T1** form (Fig. 8) were optimized using the *Quantum ESPRESSO* VC-Relax (*C*2/*c* symmetry group) method, and taking a comparable kinetic energy intercept of 65 Rydberg (Ry) (Alkorta *et al.*, 2014), as used in calculations reported in previous publications. In order to have more confidence in the results, a high convergence of 10^{-8} Ry was used in the self-consistent field (scf) calculations. The unit-cell parameters for the experimental and calculated optimized structures of the **T1** form were given in Table 5.

In addition, the total lattice energy values of both forms per unit cell were obtained using the scf method and LDA exchange-correlation. As a result of the calculations, the lattice energy values of the **T1** and **T2** forms were calculated as being −4508.43825681 and −4508.2887070 Ry, respectively. In this case, the calculations made using the periodic boundary conditions in the crystal phase show that the **T1** form has a more stable structure than the **T2** form.

4. Conclusions

In this study, the structure of 2-[2-(3-methylbenzylidene)-hydrazinyl]-4-(3-methyl-3-phenylcyclobutyl)thiazole was examined by X-ray diffraction and IR and NMR spectroscopic methods. It was observed that in both the experimental studies and the theoretical calculations, the **T1** structure was more stable than the **T2** structure. Furthermore, the energy difference between the HOMO and LUMO frontier orbitals of the two forms was calculated as 3.85 and 3.82 eV, respectively, and the larger energy range of the **T1** form as compared to the **T2** form indicates that it is more stable. As a result, all the calculations show that the **T1** form is more stable and more compatible with the structure obtained by X-ray diffraction.

Acknowledgements

I wish to thank Professor Alaaddin Cukurovali for his help with the synthesized crystal and Professor İbrahim Kani for his help with the data collection. In addition, the numerical calculations reported in this paper were fully/partially performed at TUBITAK ULAKBIM, High Performance and Grid Computing Centre (TRUBA resources).

References

Akhmedov, M. A., Sardarov, I. K., Akhmedov, I. M., Kostikov, R. R., Kisin, A. V. & Babaev, N. M. (1991). *Zh. Org. Khim.* **27**, 1434–1440.
Alkorta, I., Claramunt, R. M., Elguero, J., Ferraro, M. B., Facelli, J. C., d'Provasi, P. F. & Reviriego, F. (2014). *J. Mol. Struct.* **1075**, 551–558.
Allen, F. H. (1984). *Acta Cryst.* B**40**, 64–72.
Atkins, P. (2006). In *Atkins' Physical Chemistry*. New York: WH Freeman and Company.
Ayhan-Kılcıgil, G., Kus, C., Özdamar, E. D., Can–Eke, B. & Iscan, M. (2007). *Arch. Pharm.* **340**, 607–611.
Becke, A. D. (1993). *J. Chem. Phys.* **98**, 5648–5652.
Bruker (2008). *APEX2* and *SAINT*. Bruker AXS Inc., Madison, Wisconsin, USA.
Dennington, R., Keith, T., Millam, J., Eppinnett, K., Hovell, W. L. & Gilliland, R. (2009). *GaussView*. Version 5. Semichem Inc., Shawnee Mission, Kansas, USA.
Dolomanov, O. V., Bourhis, L. J., Gildea, R. J., Howard, J. A. K. & Puschmann, H. (2009). *J. Appl. Cryst.* **42**, 339–341.
Foresman, J. B. & Frisch, A. (1996). In *Exploring Chemistry with Electronic Structure Methods*, 2nd ed. Gaussian Inc., Pittsburgh, USA.
Frisch, M. J., *et al.* (2009). *GAUSSIAN09*. Gaussian Inc., Wallingford, CT, USA. http://www.gaussian.com.
Giannozzi, P., Baroni, S., Bonini, N., Calandra, M., Car, R., Cavazzoni, C., Ceresoli, D., Chiarotti, G. L., Cococcioni, M. & Dabo, I. (2009). *J. Phys. Condens. Matter*, **21**, 395502.
Hadjipavlou-Litina, D. & Geronikaki, A. (1996). *Arzneimittel-forschung*, **46**, 805–808.
Hart, H. (1995). In *Organic Chemistry – A Short Course*, edited by D. J. Hart & L. E. Craine. Boston: Houghton Mifflin Company.
Hohenberg, P. & Kohn, W. (1964). *Phys. Rev.* **136**, B864.
Holla, B. S., Malini, K., Rao, B. S., Sarojini, B. & Kumari, N. S. (2003). *Eur. J. Med. Chem.* **38**, 313–318.
Issaadi, S., Douadi, T., Zouaoui, A., Chafaa, S., Khan, M. & Bouet, G. (2011). *Corros. Sci.* **53**, 1484–1488.
Jarahpour, A., Motamedifar, M., Pakshir, K., Hadi, N. & Zarei, M. (2004). *Molecules*, **10**, 815–824.

Karakurt, T., Cukurovali, A., Subasi, N. T. & Kani, I. (2016). *J. Mol. Struct.* **1125**, 433–442.
Karakurt, T., Cukurovali, A., Subasi, N. T., Onaran, A., Ece, A., Eker, S. & Kani, I. (2018). *Chem. Phys. Lett.* **693**, 132–145.
Kohn, W. (1965). *Phys. Rev.* **140**, A1133.
Kus, C., Ayhan-Kilcigil, G. & Eke, B. C. (2004). *Arch. Pharm. Res.* **27**, 156–163.
Kutter, E., Machleidt, H., Reuter, W., Sauter, R. & Wildfeuer, A. (1972). *Adv. Chem. Ser.* **114**, 98–114.
Lee, C., Yang, W. & Parr, R. G. (1988). *Phys. Rev. B*, **37**, 785–789.
Macho, V., Králik, M., Hudec, J. & Cingelova, J. (2004). *J. Mol. Catal. A Chem.* **209**, 69–73.
Macrae, C. F., Bruno, I. J., Chisholm, J. A., Edgington, P. R., McCabe, P., Pidcock, E., Rodriguez-Monge, L., Taylor, R., van de Streek, J. & Wood, P. A. (2008). *J. Appl. Cryst.* **41**, 466–470.
Nagatomi, H. & Ando, K. (1984). *Arzneimittelforschung*, **34**, 599–603.
O'Neil, M. J., Smith, A. & Heckelman, P. (2001). *The Merck Index*, 13th ed. Merck & Co. Inc., Whitehouse Station, NJ, USA.
Özdemir, N. (2013). *J. Mol. Model.* **19**, 397–406.
Perdew, J. (1981). *Phys. Rev. B*, **23**, 5048.
Reddy, K. H., Reddy, P. S. & Babu, P. R. (2000). *Transition Met. Chem.* **25**, 505–510.
Sheldrick, G. M. (2015*a*). *Acta Cryst.* A**71**, 3–8.
Sheldrick, G. M. (2015*b*). *Acta Cryst.* C**71**, 3–8.
Shyam, R. & Tiwari, I. (1975). *Agric. Biol. Chem.* **39**, 715–717.
Swenson, D. C., Yamamoto, M. & Burton, D. J. (1997). *Acta Cryst.* C**53**, 1445–1447.
Zollinger, H. (2003). In *Color Chemistry: Syntheses, Properties, and Applications of Organic Dyes and Pigments*. New York: John Wiley & Sons.

supporting information

Acta Cryst. (2018). C**74** [https://doi.org/10.1107/S2053229618013475]

Investigation of the molecular structure of 4-(3-methyl-3-phenylcyclobutyl)-2-[2-(3-methylbenzylidene)hydrazinyl]thiazole in the gas and solid phases

Tuncay Karakurt

Computing details

Data collection: *APEX2* (Bruker, 2008); cell refinement: *SAINT* (Bruker, 2008); data reduction: *SAINT* (Bruker, 2008); program(s) used to solve structure: SHELXT2014 (Sheldrick, 2015a); program(s) used to refine structure: *SHELXL2016* (Sheldrick, 2015b); molecular graphics: *Mercury* (Macrae *et al.*, 2008); software used to prepare material for publication: OLEX2 (Dolomanov *et al.*, 2009).

4-(3-Methyl-3-phenylcyclobutyl)-2-[2-(3-methylbenzylidene)hydrazinyl]thiazole

Crystal data

$C_{22}H_{23}N_3S$
$M_r = 361.49$
Monoclinic, $C2/c$
$a = 20.135$ (6) Å
$b = 6.826$ (2) Å
$c = 29.027$ (9) Å
$\beta = 100.759$ (14)°
$V = 3920$ (2) Å^3
$Z = 8$
$F(000) = 1536$
$D_x = 1.225$ Mg m^{-3}
Mo $K\alpha$ radiation, $\lambda = 0.71073$ Å
Cell parameters from 9110 reflections
$\theta = 2.3$–27.5°
$\mu = 0.18$ mm^{-1}
$T = 296$ K
Yellow, square
0.30 × 0.25 × 0.20 mm

Data collection

Bruker APEXII CCD area-detector diffractometer
phi and ω scans
37086 measured reflections
4808 independent reflections
3768 reflections with $I > 2\sigma(I)$
$R_{int} = 0.030$
$\theta_{max} = 28.5°$, $\theta_{min} = 2.1°$
$h = -26\rightarrow23$
$k = -8\rightarrow9$
$l = -38\rightarrow38$

Refinement

Refinement on F^2
Least-squares matrix: full
$R[F^2 > 2\sigma(F^2)] = 0.053$
$wR(F^2) = 0.139$
$S = 1.07$
4808 reflections
241 parameters
0 restraints
Primary atom site location: structure-invariant direct methods
Secondary atom site location: difference Fourier map
Hydrogen site location: mixed
H atoms treated by a mixture of independent and constrained refinement
$w = 1/[\sigma^2(F_o^2) + (0.0587P)^2 + 3.2259P]$ where $P = (F_o^2 + 2F_c^2)/3$
$(\Delta/\sigma)_{max} = 0.001$
$\Delta\rho_{max} = 0.26$ e Å^{-3}
$\Delta\rho_{min} = -0.22$ e Å^{-3}

Special details

Geometry. All esds (except the esd in the dihedral angle between two l.s. planes) are estimated using the full covariance matrix. The cell esds are taken into account individually in the estimation of esds in distances, angles and torsion angles; correlations between esds in cell parameters are only used when they are defined by crystal symmetry. An approximate (isotropic) treatment of cell esds is used for estimating esds involving l.s. planes.

Fractional atomic coordinates and isotropic or equivalent isotropic displacement parameters (Å²)

	x	*y*	*z*	U_{iso}*/U_{eq}
S1	0.58902 (2)	0.56865 (8)	0.48351 (2)	0.05323 (16)
N1	0.70748 (7)	0.4780 (2)	0.46802 (5)	0.0422 (3)
N3	0.60750 (7)	0.2186 (2)	0.53558 (5)	0.0476 (4)
N2	0.65668 (8)	0.2373 (2)	0.50859 (6)	0.0487 (4)
C12	0.69121 (8)	0.6635 (3)	0.44866 (6)	0.0424 (4)
C14	0.65816 (8)	0.4144 (3)	0.48732 (6)	0.0424 (4)
C7	0.74959 (9)	0.9158 (3)	0.35970 (6)	0.0455 (4)
C10	0.73941 (9)	0.7662 (3)	0.42417 (6)	0.0438 (4)
H10	0.784422	0.768443	0.444097	0.053*
C9	0.72094 (10)	0.9717 (3)	0.40406 (6)	0.0460 (4)
H9A	0.745584	1.076540	0.422312	0.055*
H9B	0.672748	0.998004	0.397767	0.055*
C1	0.70844 (9)	0.9818 (3)	0.31335 (6)	0.0506 (5)
C15	0.59881 (9)	0.0498 (3)	0.55155 (7)	0.0513 (4)
H15	0.623028	−0.055860	0.543012	0.062*
C13	0.63081 (9)	0.7336 (3)	0.45386 (6)	0.0498 (4)
H13	0.613674	0.854947	0.442950	0.060*
C11	0.74476 (10)	0.6988 (3)	0.37375 (6)	0.0512 (4)
H11A	0.785119	0.623283	0.372290	0.061*
H11B	0.704628	0.632721	0.357270	0.061*
C16	0.55110 (9)	0.0188 (3)	0.58330 (7)	0.0519 (5)
C17	0.53565 (9)	0.1666 (3)	0.61245 (7)	0.0561 (5)
H17	0.553888	0.290805	0.610552	0.067*
C8	0.82230 (10)	0.9849 (4)	0.36365 (7)	0.0631 (6)
H8A	0.823214	1.125294	0.361829	0.095*
H8B	0.841166	0.930028	0.338492	0.095*
H8C	0.848384	0.943057	0.393122	0.095*
C2	0.68400 (11)	1.1711 (4)	0.30784 (8)	0.0654 (6)
H2A	0.693676	1.258780	0.332708	0.079*
C18	0.49354 (10)	0.1324 (4)	0.64436 (7)	0.0677 (6)
C6	0.69462 (12)	0.8568 (4)	0.27516 (7)	0.0684 (6)
H6	0.711498	0.729665	0.277792	0.082*
C22	0.52187 (12)	−0.1646 (4)	0.58526 (9)	0.0716 (6)
H22	0.531490	−0.265086	0.565886	0.086*
C20	0.46580 (11)	−0.0527 (5)	0.64543 (9)	0.0822 (8)
H20	0.437762	−0.078927	0.666763	0.099*
C5	0.65620 (15)	0.9183 (6)	0.23331 (8)	0.0923 (9)
H5	0.647496	0.832394	0.208031	0.111*
C21	0.47859 (13)	−0.1969 (5)	0.61603 (11)	0.0870 (8)

H21	0.457949	−0.318478	0.616694	0.104*
C3	0.64509 (13)	1.2321 (4)	0.26558 (10)	0.0848 (8)
H3	0.628690	1.359669	0.262285	0.102*
C4	0.63096 (14)	1.1029 (6)	0.22863 (10)	0.0963 (10)
H4	0.604147	1.142175	0.200516	0.116*
C19	0.47894 (17)	0.2921 (6)	0.67679 (10)	0.1083 (11)
H19A	0.516064	0.382644	0.682282	0.162*
H19B	0.472999	0.235628	0.706034	0.162*
H19C	0.438443	0.359962	0.662735	0.162*
H2	0.6956 (12)	0.156 (3)	0.5147 (7)	0.063 (6)*

Atomic displacement parameters (Å²)

	U^{11}	U^{22}	U^{33}	U^{12}	U^{13}	U^{23}
S1	0.0409 (2)	0.0575 (3)	0.0635 (3)	0.0010 (2)	0.0154 (2)	0.0054 (2)
N1	0.0404 (7)	0.0455 (8)	0.0417 (7)	−0.0034 (6)	0.0100 (6)	0.0008 (6)
N3	0.0419 (8)	0.0524 (9)	0.0505 (8)	−0.0037 (7)	0.0143 (6)	0.0032 (7)
N2	0.0448 (8)	0.0480 (9)	0.0571 (9)	−0.0021 (7)	0.0193 (7)	0.0046 (7)
C12	0.0415 (9)	0.0480 (10)	0.0361 (8)	−0.0021 (7)	0.0031 (7)	0.0003 (7)
C14	0.0396 (8)	0.0483 (10)	0.0392 (8)	−0.0045 (7)	0.0071 (7)	−0.0052 (7)
C7	0.0447 (9)	0.0534 (10)	0.0383 (8)	−0.0092 (8)	0.0076 (7)	−0.0015 (8)
C10	0.0416 (9)	0.0495 (10)	0.0394 (8)	−0.0040 (7)	0.0055 (7)	0.0006 (7)
C9	0.0546 (10)	0.0447 (10)	0.0390 (9)	−0.0066 (8)	0.0089 (7)	−0.0015 (7)
C1	0.0434 (9)	0.0692 (13)	0.0396 (9)	−0.0152 (9)	0.0091 (7)	0.0047 (8)
C15	0.0450 (10)	0.0510 (11)	0.0594 (11)	−0.0044 (8)	0.0138 (8)	0.0019 (9)
C13	0.0464 (10)	0.0518 (11)	0.0508 (10)	0.0014 (8)	0.0077 (8)	0.0075 (8)
C11	0.0565 (11)	0.0508 (11)	0.0482 (10)	−0.0031 (8)	0.0151 (8)	−0.0037 (8)
C16	0.0379 (9)	0.0629 (12)	0.0550 (11)	−0.0043 (8)	0.0086 (8)	0.0107 (9)
C17	0.0390 (9)	0.0749 (14)	0.0538 (11)	−0.0008 (9)	0.0072 (8)	0.0135 (10)
C8	0.0488 (11)	0.0813 (15)	0.0575 (12)	−0.0114 (10)	0.0058 (9)	0.0056 (11)
C2	0.0671 (13)	0.0688 (14)	0.0587 (12)	−0.0125 (11)	0.0076 (10)	0.0155 (11)
C18	0.0431 (10)	0.1099 (19)	0.0509 (11)	0.0090 (12)	0.0105 (9)	0.0191 (12)
C6	0.0653 (13)	0.0923 (17)	0.0469 (11)	−0.0110 (12)	0.0087 (10)	−0.0096 (11)
C22	0.0629 (13)	0.0709 (15)	0.0829 (16)	−0.0151 (11)	0.0190 (12)	0.0136 (12)
C20	0.0481 (12)	0.132 (2)	0.0695 (15)	−0.0040 (14)	0.0182 (11)	0.0417 (16)
C5	0.0819 (18)	0.145 (3)	0.0450 (12)	−0.0263 (19)	−0.0007 (12)	−0.0066 (16)
C21	0.0658 (15)	0.099 (2)	0.099 (2)	−0.0225 (14)	0.0208 (14)	0.0323 (17)
C3	0.0689 (15)	0.0942 (19)	0.0875 (18)	−0.0076 (14)	0.0053 (13)	0.0429 (16)
C4	0.0670 (16)	0.153 (3)	0.0607 (15)	−0.0277 (19)	−0.0087 (12)	0.0318 (18)
C19	0.100 (2)	0.156 (3)	0.0807 (18)	0.020 (2)	0.0474 (17)	0.006 (2)

Geometric parameters (Å, º)

S1—C13	1.728 (2)	C16—C17	1.389 (3)
S1—C14	1.7325 (19)	C16—C22	1.389 (3)
N1—C14	1.302 (2)	C17—C18	1.387 (3)
N1—C12	1.400 (2)	C17—H17	0.9300
N3—C15	1.266 (2)	C8—H8A	0.9600

N3—N2	1.378 (2)	C8—H8B	0.9600
N2—C14	1.361 (2)	C8—H8C	0.9600
N2—H2	0.95 (2)	C2—C3	1.390 (3)
C12—C13	1.341 (3)	C2—H2A	0.9300
C12—C10	1.482 (2)	C18—C20	1.384 (4)
C7—C1	1.511 (3)	C18—C19	1.505 (4)
C7—C8	1.522 (3)	C6—C5	1.378 (4)
C7—C11	1.544 (3)	C6—H6	0.9300
C7—C9	1.554 (2)	C22—C21	1.377 (3)
C10—C9	1.539 (3)	C22—H22	0.9300
C10—C11	1.557 (2)	C20—C21	1.359 (4)
C10—H10	0.9800	C20—H20	0.9300
C9—H9A	0.9700	C5—C4	1.356 (5)
C9—H9B	0.9700	C5—H5	0.9300
C1—C2	1.381 (3)	C21—H21	0.9300
C1—C6	1.385 (3)	C3—C4	1.376 (4)
C15—C16	1.466 (3)	C3—H3	0.9300
C15—H15	0.9300	C4—H4	0.9300
C13—H13	0.9300	C19—H19A	0.9600
C11—H11A	0.9700	C19—H19B	0.9600
C11—H11B	0.9700	C19—H19C	0.9600

C13—S1—C14	88.15 (9)	C17—C16—C22	119.00 (19)
C14—N1—C12	109.52 (15)	C17—C16—C15	121.74 (18)
C15—N3—N2	117.07 (16)	C22—C16—C15	119.2 (2)
C14—N2—N3	114.77 (15)	C18—C17—C16	121.3 (2)
C14—N2—H2	121.0 (13)	C18—C17—H17	119.4
N3—N2—H2	119.8 (13)	C16—C17—H17	119.4
C13—C12—N1	115.25 (16)	C7—C8—H8A	109.5
C13—C12—C10	125.06 (17)	C7—C8—H8B	109.5
N1—C12—C10	119.68 (15)	H8A—C8—H8B	109.5
N1—C14—N2	125.06 (16)	C7—C8—H8C	109.5
N1—C14—S1	115.99 (14)	H8A—C8—H8C	109.5
N2—C14—S1	118.93 (13)	H8B—C8—H8C	109.5
C1—C7—C8	109.54 (15)	C1—C2—C3	120.8 (2)
C1—C7—C11	118.03 (15)	C1—C2—H2A	119.6
C8—C7—C11	112.62 (17)	C3—C2—H2A	119.6
C1—C7—C9	115.98 (16)	C20—C18—C17	117.9 (2)
C8—C7—C9	111.24 (15)	C20—C18—C19	121.4 (2)
C11—C7—C9	88.01 (13)	C17—C18—C19	120.7 (3)
C12—C10—C9	118.65 (15)	C5—C6—C1	120.9 (3)
C12—C10—C11	118.54 (15)	C5—C6—H6	119.5
C9—C10—C11	88.10 (13)	C1—C6—H6	119.5
C12—C10—H10	109.9	C21—C22—C16	119.7 (3)
C9—C10—H10	109.9	C21—C22—H22	120.2
C11—C10—H10	109.9	C16—C22—H22	120.2
C10—C9—C7	89.40 (14)	C21—C20—C18	121.5 (2)
C10—C9—H9A	113.7	C21—C20—H20	119.2

C7—C9—H9A	113.7	C18—C20—H20	119.2
C10—C9—H9B	113.7	C4—C5—C6	120.6 (3)
C7—C9—H9B	113.7	C4—C5—H5	119.7
H9A—C9—H9B	111.0	C6—C5—H5	119.7
C2—C1—C6	118.0 (2)	C20—C21—C22	120.6 (3)
C2—C1—C7	120.40 (18)	C20—C21—H21	119.7
C6—C1—C7	121.6 (2)	C22—C21—H21	119.7
N3—C15—C16	120.89 (18)	C4—C3—C2	119.7 (3)
N3—C15—H15	119.6	C4—C3—H3	120.1
C16—C15—H15	119.6	C2—C3—H3	120.1
C12—C13—S1	111.09 (15)	C5—C4—C3	119.9 (3)
C12—C13—H13	124.5	C5—C4—H4	120.1
S1—C13—H13	124.5	C3—C4—H4	120.1
C7—C11—C10	89.07 (13)	C18—C19—H19A	109.5
C7—C11—H11A	113.8	C18—C19—H19B	109.5
C10—C11—H11A	113.8	H19A—C19—H19B	109.5
C7—C11—H11B	113.8	C18—C19—H19C	109.5
C10—C11—H11B	113.8	H19A—C19—H19C	109.5
H11A—C11—H11B	111.0	H19B—C19—H19C	109.5

C15—N3—N2—C14	171.86 (16)	C14—S1—C13—C12	0.56 (15)
C14—N1—C12—C13	0.0 (2)	C1—C7—C11—C10	−135.92 (16)
C14—N1—C12—C10	−179.40 (14)	C8—C7—C11—C10	94.86 (17)
C12—N1—C14—N2	178.65 (16)	C9—C7—C11—C10	−17.36 (13)
C12—N1—C14—S1	0.47 (18)	C12—C10—C11—C7	139.41 (16)
N3—N2—C14—N1	165.93 (16)	C9—C10—C11—C7	17.54 (14)
N3—N2—C14—S1	−15.9 (2)	N3—C15—C16—C17	−27.8 (3)
C13—S1—C14—N1	−0.61 (14)	N3—C15—C16—C22	154.0 (2)
C13—S1—C14—N2	−178.91 (15)	C22—C16—C17—C18	2.1 (3)
C13—C12—C10—C9	1.9 (3)	C15—C16—C17—C18	−176.13 (18)
N1—C12—C10—C9	−178.81 (14)	C6—C1—C2—C3	1.8 (3)
C13—C12—C10—C11	−102.9 (2)	C7—C1—C2—C3	−178.87 (19)
N1—C12—C10—C11	76.5 (2)	C16—C17—C18—C20	−1.7 (3)
C12—C10—C9—C7	−139.20 (15)	C16—C17—C18—C19	178.1 (2)
C11—C10—C9—C7	−17.43 (13)	C2—C1—C6—C5	−1.6 (3)
C1—C7—C9—C10	137.98 (16)	C7—C1—C6—C5	179.1 (2)
C8—C7—C9—C10	−95.97 (17)	C17—C16—C22—C21	−0.3 (3)
C11—C7—C9—C10	17.58 (13)	C15—C16—C22—C21	178.0 (2)
C8—C7—C1—C2	−80.5 (2)	C17—C18—C20—C21	−0.6 (3)
C11—C7—C1—C2	148.82 (18)	C19—C18—C20—C21	179.7 (3)
C9—C7—C1—C2	46.4 (2)	C1—C6—C5—C4	−0.1 (4)
C8—C7—C1—C6	98.8 (2)	C18—C20—C21—C22	2.4 (4)
C11—C7—C1—C6	−31.8 (3)	C16—C22—C21—C20	−1.9 (4)
C9—C7—C1—C6	−134.30 (19)	C1—C2—C3—C4	−0.3 (4)
N2—N3—C15—C16	175.61 (16)	C6—C5—C4—C3	1.6 (4)
N1—C12—C13—S1	−0.4 (2)	C2—C3—C4—C5	−1.4 (4)
C10—C12—C13—S1	178.91 (13)		